Atmospheric Environment 147 (2016) 296–309

Contents lists available at ScienceDirect

Atmospheric Environment

journal homepage: www.elsevier.com/locate/atmosenv

Effects of meteorological conditions on sulfur dioxide air pollution in the North China plain during winters of 2006–2015

Chase Calkins [a, b], Cui Ge [a, b], Jun Wang [a, b, *], Mark Anderson [a], Kai Yang [c]

[a] Department of Earth and Atmospheric Sciences, University of Nebraska, Lincoln, NE 68588, United States
[b] Center for Global and Regional Environmental Studies, Department of Chemical and Biochemical Engineering, University of Iowa, Iowa City, IA 52242, United States
[c] Department of Atmospheric and Oceanic Science, University of Maryland, College Park, MD 20742, United States

HIGHLIGHTS

- Meteorological conditions with OMI-based high SO_2 days in China are studied.
- Climatological anomaly of meteorological variables in high SO_2 days are quantified.
- Year-to-year winter change of columnar SO_2 distribution is mostly due to SO_2 emission.
- Surface SO_2 distribution has stronger dependence on meteorology than columnar SO2.
- Columnar SO_2 climatology is not representative to surface SO_2 climatology.

ARTICLE INFO

Article history:
Received 8 March 2016
Received in revised form
29 September 2016
Accepted 5 October 2016
Available online 5 October 2016

Keywords:
SO_2
Air pollution meteorology and climatology
OMI
GEOS-Chem

ABSTRACT

The last decade has seen frequent occurrences of severe air pollution episodes of high loading in SO_2 during winters in the North China Plain (NCP). Using satellite data from the Ozone Monitoring Instrument (OMI), chemistry transport model (GEOS-Chem) simulations, and National Center for Environmental Predication (NCEP) meteorological reanalysis, this study examines meteorological and synoptic conditions associated with air pollution episodes during 2006–2015 winters. OMI-based SO_2 data suggest a large decrease (~30% in area average) of SO_2 emissions since 2010. Statistical analysis shows that meteorological conditions associated with the top 10% of OMI-based high SO_2 days are found on average to be controlled by high pressure systems with 2 m s^{-1} lower wind speeds, slightly warmer, 1–2 °C, temperatures and 10–20% higher relative humidities from the surface to 850 hPa. Numerical experiments with GOES-Chem nested grid simulations at 0.5° × 0.667° resolution are conducted for winters of 2009 as a control year, and 2012 and 2013 as years for sensitivity analysis. The experiments reveal that year-to-year change of winter columnar SO_2 amounts and distributions in first order are linearly proportional to the change in SO_2 emissions, regardless of the differences in meteorological conditions. In contrast, the surface SO_2 amounts and distributions exhibit highly non-linear relationships with respect to the emissions and stronger dependence on the meteorological conditions. Longer data records of atmospheric SO_2 from space combined with meteorological reanalysis are needed to further study the meteorological variations in air pollution events and the air pollution climatology in the context of climate change.

1. Introduction

Sulfur dioxide (SO_2) gas is emitted both naturally and anthropogenically through volcanic eruptions and fossil fuel combustion. Estimates by the World Health Organization (WHO, 2001) show that economic health impact (excess mortality and morbidity) due to air pollution of SO_2 is ~43.8 billion RMB Yuan (or ~6.5 billion $) in China. Smith et al. (2011) found that annual emissions of SO_2

* Corresponding author. Department of Chemical and Biochemical Engineering, 4133 Seamans Center, Iowa City, IA 52242, United States.
E-mail address: jun-wang-1@uiowa.edu (J. Wang).

http://dx.doi.org/10.1016/j.atmosenv.2016.10.005
1352-2310/

topped ~35 Teragrams (Tg) in the US and Canada, and ~41 Tg SO_2 in Western and Central Europe during the 1970s. However, in the last two decades, North America (United States and Canada) and Europe have been steadily reducing their emissions from 24 Tg to 31 Tg, respectively in 1990 to 17 Tg and 14 Tg, respectively in 2000, and to 15 Tg and 11 Tg, respectively in 2005. These decreasing trends contrast with the increasing trend of SO_2 in many developing countries; annual emissions by sector and fuel types calculated from satellite data show an increasing trend of SO_2 during 1996–2008 and decreasing thereafter in China, with a range of 30–40 Tg per year (Lu et al., 2010).

The distribution of atmospheric SO_2 not only depends on the emission of SO_2, but also is affected by meteorological conditions. Xue and Yin, 2013 found that at Shanghai, SO_2 amounts were negatively correlated with temperature, dew point, relative humidity, wind speed and positively correlated with pressure from October 2004 to September 2012. Bridgman et al. (2002) found that SO_2 surface concentrations in the Czech Republic can be influenced by strong variations of wind direction, wind speed and temperature within the seasons. In Trabzon City, Turkey, Cuhadaroglu and Demirci (1997) found that SO_2 surface concentrations when compared with humidity, wind and temperature have moderate relations in November and December while having weaker relations during January–April. However in Balikesir, Turkey, SO_2 was highly correlated with lower temperatures and lower wind speeds, and less correlated with relative humidity (Ilten and Selici, 2008).

This study investigates how meteorological factors favor high episodes of SO_2 pollution events in China through a combined use of a chemistry transport model (CTM), satellite products of SO_2, and meteorological reanalysis from the National Center for Environmental Predication (NCEP). Many satellite sensors have the capability to monitor atmospheric SO_2 from space, including Scanning Imaging Absorption Spectrometer for Atmospheric Chartography (SCIAMACHY) (Afe et al., 2004; Richter et al., 2006; Lee et al., 2008, 2009; Zhang et al., 2012), Ozone Monitoring Instrument (OMI) (Krotkov et al., 2008; Carn et al., 2015; Yang et al., 2007; He et al., 2012), and most recently Ozone Mapping and Profiler Suite (OMPS) (Yang et al., 2013). However, these satellite-based SO_2 data in the past have been primarily used for estimating SO_2 emissions and to some extent to evaluate and improve CTM simulations of atmospheric SO_2 (Lee et al., 2009, 2011; Wang et al., 2013). Yang et al. (2013) is among the few studies that have combined meteorological data and satellite SO_2 data from OMPS, to study the role of the atmosphere in an air pollution event for the 2013 winter in China. Numerous studies have also conducted ground-based observations and modeling analyses of air pollution events in China (Chan and Yao, 2008; Lu et al., 2010, 2011; Zhang et al., 2015), just to name a few.

Our study area focuses on the North China Plain (NCP) where the SO_2 emissions have changed rapidly due to the combination of fast economic growth and implementation of air pollution control policies in the last decade for this region (Li et al., 2010). However, these rapid changes of SO_2 emission, together with frequent SO_2 pollution episodes also make the NCP a unique place to combine both satellite data and CTM results to study air pollution meteorology (Yang et al., 2013). Past studies of air pollution meteorology have primarily relied on ground-based observations and numerical models (Fiore et al., 2012). Hence, our joint and new analysis of satellite and model data can reveal (to some extent) how the changing climate (including meteorological conditions) may affect SO_2 air quality, and thus have important implications for predicting future air quality as the climate continues to change (Fiore et al., 2012). The study period of focus is the meteorological winter (December, January and February) during 2006–2015. We describe the data and model in Section 2, model experiment design and approaches in Section 3, results in Section 4 and conclude the paper in Section 5.

2. Datasets and study area

Data used in this study over the NCP (110°E–125°E, 30°N-42°N, Fig. 1) include: (1) Level 3 OMI-best pixel scans, (2) hourly data from a CTM driven by the meteorology from the Goddard Earth Observing System (GEOS); and (3) reanalysis meteorological data from NCEP.

2.1. OMI SO_2

The Ozone Monitoring Instrument (OMI) is a sun-synchronous polar orbiting Dutch/Finnish sensor on the AURA satellite launched on 15 July 2004. OMI is a nadir viewing imaging spectrograph that measures backscattered solar radiation over the 264–504 nm wavelength. The first UV band is from 263 to 311 nm while the second band is from 307 to 383 nm. The absorption spectrum of SO_2 is typically between 305 and 330 nm. OMI uses the 310.8–314.4 nm wavelength to capture the SO_2 in the atmosphere. OMI's pixel size is 13 km (along the orbit) and 24 km (across the orbit) at nadir. (Levelt et al., 2006). OMI's field view of 114° corresponds to a 2600 km wide swath on the surface, which enables daily global coverage. It uses a 2-D Charge Coupled Device (CCD) that can obtain spatial and spectral data simultaneously. Beginning on 25 June 2007, the OMI sensor has been flagged for row anomalies, of which, changes over time. Row anomalies are an anomaly that affects the radiance data in all wavelengths in a particular view direction. Through 28 February 2015, rows 21–54 have been affected by this anomaly which accounts for 39% of the data.

For this study, we used the planetary boundary layer (PBL) SO_2_PBL data from the level-3 OMI/AURA SO_2 data product, OMSO2e (Version 003) (Krotkov et al., 2015) retrieved 4 May 2015, for the meteorological winter time range of 1 December 2005 to 28 February 2015. The current version of the data in the SO_2_PBL is based on a principal component analysis (PCA) of the OMI radiance data (Li et al., 2013). This differs from the band residual difference (BRD) retrieval (Krotkov et al., 2005), as data in high latitudes tend to have larger noise and biases. The OMI SO2 product has been validated over China (Krotkov et al., 2015). The current version of OMI SO2e contains the best pixel of the data. These data have been screened for OMI row anomaly and other data quality flags. During the available 900 days of data, only 870 days contained data. SO_2 accuracy depends on two components: the uncertainty in slant column density (SCD) and the average photon path, characterized by the error in assumed air mass factor (AMF). Also, depending on vertical distribution, aerosols and sub pixel clouds affect AMF.

2.2. GEOS–Chem model

The global chemical transport model GEOS-Chem (v9-01-03) is driven by the Goddard Earth Observing System (GEOS) (Bey et al., 2001) of the NASA Global Modeling and Assimilation Office (GMAO). We use GEOS-Chem for a three-month simulation during the winter months of sulfate aerosols with a spin up of one month with full chemistry. Assimilated meteorological fields from GEOS of NASA Global Modeling Assimilation Office are used to drive GEOS-Chem (Park et al., 2004). The model uses GEOS-5 meteorological fields with 47 vertical levels initially ran at 4° latitude by 5° longitude and then in a nested run at 0.5° latitude by 0.667° longitude. The bottom model layer is ~100 m thick above the surface. The temporal resolution is a six hour average for 3-D meteorological variables and a three hour average for 2-D variables.

The global anthropogenic emissions for NO_x, SO_x, and CO are

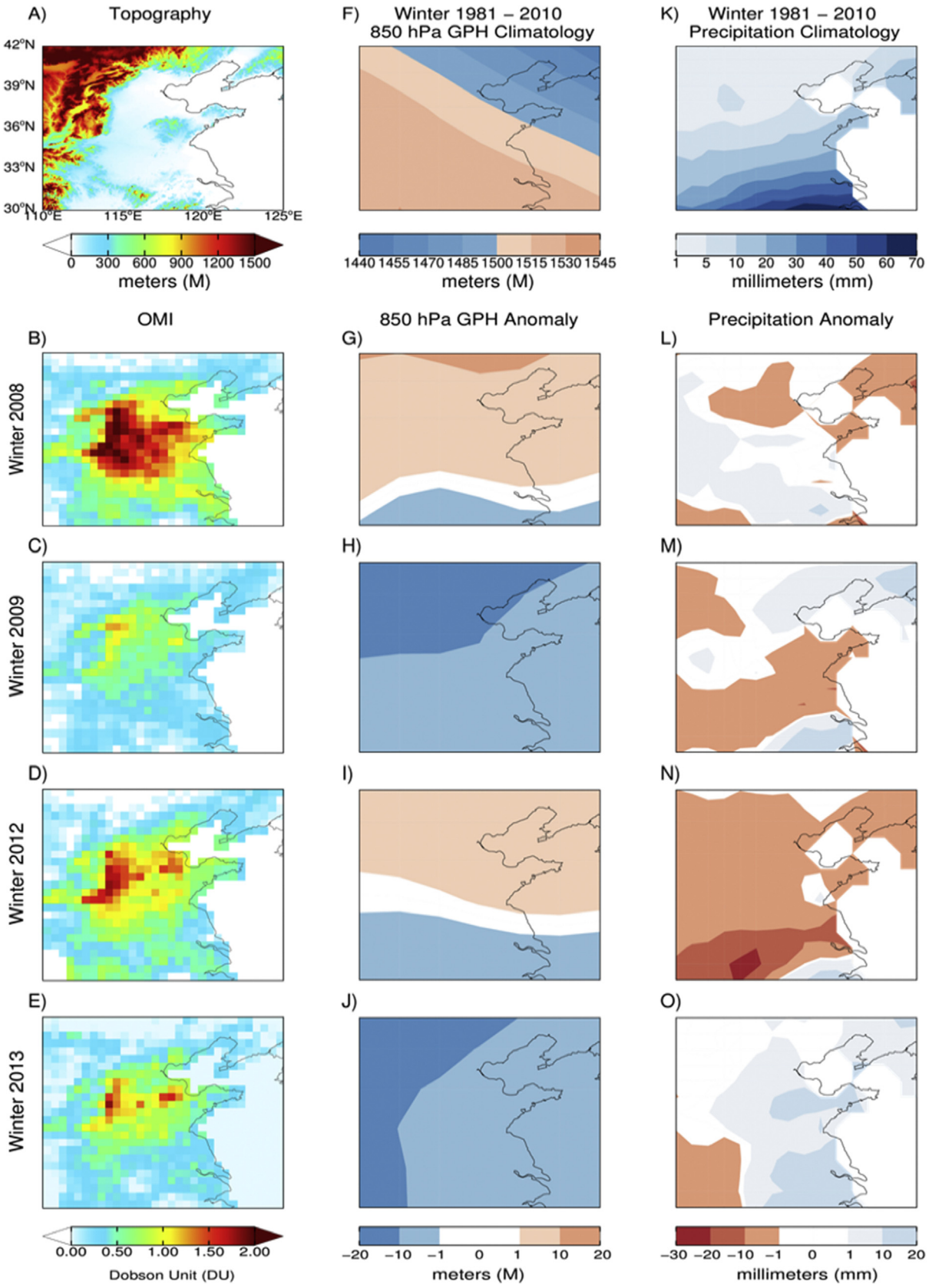

Fig. 1. For comparison purposes the topography of the North China Plain (A), winter climatology (1981–2010) of heights at 850 hPa (F) and precipitation (K) are shown at top. Also shown are the winter average SO_2 columnar loading for OMI (B–E), GPH anomaly (G–J) and precipitation anomaly (L–O) for the winters of 2008 (second row from the top), 2009 (third row), 2012 (fourth row) and 2013 (fifth row).

based on the Emissions Database for Global Atmospheric Research (EDGAR) emission database (Olivier and Berdowski, 2001). The global emission is replaced by Streets 2006 emissions (Zhang et al., 2009) from the Intercontinental Chemical Transport Experiment-Phase B (INTEX-B) aircraft mission for the nested model run. The INTEX-B mission represented 22 different countries for the year 2006 with a spatial resolution of 30 min by 30 min done monthly. However, when this inventory was developed in 2006 and 2007, most of the available statistics for Chinese provinces were for the 2004 and 2005 years with the exception of a few 2006. This dataset was then extrapolated to 2006 based on various fast track statistics that were published monthly. For China, the 2006 national emission total for SO_2 is ~31 Tg/year. The convection and transport time step of our model is set to 30 min and the emission time step is set to 60 min for the 4° latitude by 5° longitude resolution, while the nested grid is run at 10 min and 20 min, respectively.

2.3. Meteorological reanalysis data

The meteorological data used for studying the change of large scale dynamics and meteorological conditions are from NCEP reanalysis data, which are available from January 1948 – present. We did not use the GEOS meteorological data to study the meteorological anomalies because of its short record that does not cover the time period (1981–2010) used in this study for computing climatological means of all meteorological variables, (although we note that Modern-Era Retrospective analysis for Research and Applications (MERRA), Version 2, or MERRA-2 data were released after this study started and covers the time period of 1981–2010, http://gmao.gsfc.nasa.gov/reanalysis/MERRA-2/docs/). The NCEP reanalysis data are reported daily. Daily and monthly composites are available from the National Oceanic and Atmospheric Administration (NOAA) Earth System Research Laboratory (ESRL) (Kalnay et al., 1996) physical science data (PSD), Boulder, Colorado, USA from their Web site http://www.esrl.noaa.gov/psd/. The variables used for this study are 850 hPa temperature, 850 hPa relative humidity, 850 hPa height, 850 hPa U and V wind vector components to make wind speeds and surface pressure. The current version of the data were accessed on 13 August 2015.

3. Data processing, and experiment design

3.1. OMI data processing for analyzing air pollution meteorology

Daily retrievals from OMI, allocated to grid cells of 0.25° × 0.25°, were filtered with a large solar zenith angle and viewing zenith angle greater than 70°. To further ensure data quality, only SO_2 data retrieved with low radiative cloud fractions, less than 0.2, are used in this study. First, we re-grid daily OMI SO_2 into a 2.5° by 2.5° mesh to match the resolution of the NCEP reanalysis data. Second, for each grid box, we sort the OMI SO_2 data from the highest to the lowest loadings during the winters of 2006–2015, and then index the days that have SO_2 loading in the top 10 percentile of all valid OMI SO_2 data for that grid box; hereafter these days are called extreme SO_2 days. Third, meteorological conditions (from NCEP) on the extreme SO_2 days are averaged for each grid box; the combination of averaged parameters in each of the grid boxes yields the typical meteorological conditions for high SO_2 loadings. Since SO_2 loadings are primarily located within the planetary boundary layer, we focus on the analyses of the meteorological conditions in the lower troposphere at the 850 hPa level.

To generate monthly distributions of SO_2, OMI SO_2 data are also re-gridded into a spatial resolution at 0.5° by 0.5° to be comparable to the resolution of GEOS-Chem nested grid resolution and also to ensure that we have enough data samples in each grid box to capture the regional scale of SO_2 climatology. A minimum of five days of available SO_2 data per grid box are required to compute the monthly mean of SO_2 for that grid box. These monthly gridded SO_2 data in the first (2006–2010) and second (2011–2015) five year periods are also added together to create a map with a minimum of 75 days per grid box to create five year averages of SO_2. The decadal averages are computed by averaging the ten years of data with a minimum of 150 one hundred and fifty days per grid box.

3.2. GEOS-Chem simulation and experiment design

Various GEOS-Chem simulations are conducted to analyze the change of atmospheric SO_2 due to the change of emissions and/or meteorological conditions. The first set of simulations are run with the same default emissions for winters 2009, 2012 and 2013, thereby enabling the analysis of the response of atmospheric SO_2 to the change of meteorological conditions. These years (2009, 2012, and 2013) are selected to be representative of normal, wet, and dry years respectively (in terms of total precipitation in our study region). The second set of simulations is the same as the first set, however, emissions are reduced by 50%. Contrast analysis between the first and second set of simulations of the same year can reveal if the reduction of SO_2 emissions by 50% leads to the overall decrease of atmospheric SO_2 by 50%, and how such a reduction may change spatially. In addition, with these two sets of simulations, we can also analyze the change of a SO_2 episode (in terms of peak of atmospheric SO_2 amount) due to the change of emissions, meteorological conditions, or combined effects.

4. Results

4.1. Overview

The NCP is flat with topography less than 100 m, (Fig. 1A). However, the Taihang mountain range, located to the west of the NCP can extend higher than 1500 m. Fig. 2B also shows the locations of each province in our study region. During the winter months, the climatological average (1981–2010) for the 850 hPa height ranges from 1440 geopotential meters (gpm) in the northeastern part of the study region to 1530 gpm in the southwestern part, with major cities like Beijing near 1490 gpm and Shanghai near 1515 gpm (Fig. 1F). The standard 850 hPa height is 1500 gpm, the meteorological conditions conducted over the mountains are less realistic, since they could be below the surface. The precipitation climatological average during winter is relatively dry in the northern part of the plains, with Beijing receiving less than 5 mm, Shanghai around 35 mm, and the southern part of the plains receiving around 70 mm (Fig. 1K).

To determine the meteorological patterns for high and low loading years, four years were investigated including; two high years, winter 2008 (Fig. 1B) and winter 2012 (Fig. 1D), one intermediate year, winter 2013 (Fig. 1E) and one low year, winter 2009 (Fig. 1C). The highest SO_2 loading event came in winter 2008. Areas of high loadings are characterized by OMI SO_2 values of greater than 0.5 DU. There are distinct areas east of the Taihang mountain range that are continuously exceeding 0.5 DU. However, the loadings seen in winters 2009, 2012 and 2013 are not as heavily polluted as winter 2008 loadings, though there are similarities in areas. There is a clear boundary of higher loading that forms east of the Taihang mountain range. The high SO_2 loadings observed in winter 2008 can be attributed partially to higher heights at the 850 hPa level, around 10 gpm, above the climatological average (Fig. 1G). Precipitation is generally near normal or slightly drier in the same area (Fig. 1L). The relatively drier area is also where precipitation is less than 5 mm on average. Regions of higher heights and drier

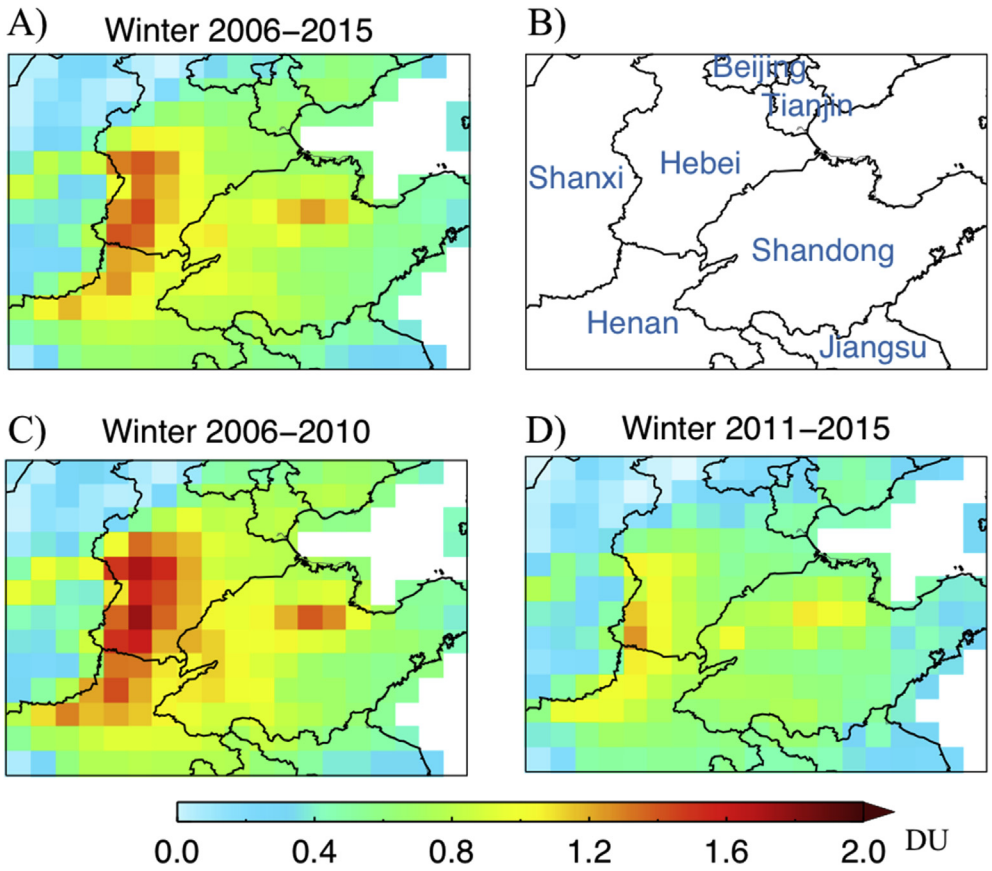

Fig. 2. Average OMI SO_2 amount for winters (A) 2006–2015, (C) 2006–2015, and (D) 2011–2015 re-gridded to 0.5° × 0.5°. (B) Shows the map of different Chinese provinces in the study region.

conditions will generally lead to higher SO_2 loadings. Winter 2009, our GEOS-Chem control year, saw lower heights, around 10 to 20 gpm (Fig. 1H), and precipitation was near normal or slightly wetter (Fig. 1M), leading to a decrease in SO_2 loadings.

The other high loading year, winter 2012, is similar in loading regions observed in winter 2008. The region still sees values greater than 0.5 DU, however, winter 2012 loadings are generally lower than those found during 2008. Winter 2013 is classified as an intermediate year, because winter 2013 loadings are between winter 2012 and winter 2009.

In winter 2012, the 850 hPa height anomalies (Fig. 1I) are similar to those of winter 2008 (Fig. 1G) with the SO_2 loadings being in regions of higher heights, around 10 gpm above normal. Precipitation in winter 2012 (Fig. 1N) is much drier compared to winter 2008 (Fig. 1L), leading us to assume that winter 2012 should be as high, or more severe of a loading event than winter 2008. However, there is a significant decrease in SO_2 loading over the region compared to winter 2008. The decrease was caused by January 2012 850 hPa heights, as they were near normal to 10 gpm below the climatological average and February 2008 was 20 gpm above climatology. The December months are similar to each other and cancel each other out (not shown). In winter 2013, height anomalies (Fig. 1J) are similar to winter 2009 (Fig. 1H) with the loadings in an area of 10 gpm less than the climatological average. Between the two years, precipitation is the main difference. Precipitation in winter 2013 is wetter, around 10–20 mm more than the climatological average (Fig. 1O) and winter 2009 (Fig. 1M) varies between −10 and 10 mm. We expect winter 2013 loadings to look like winter 2009 or have lower SO_2 loadings based the same heights and more precipitation, however, there are regions of higher loadings. Winter 2009 is lower in loadings because February 2009 heights were 20–30 gpm less than the climatological average while the December and January height field canceled each other out (not shown).

Generally speaking, higher heights will lead to an increase in SO_2 loadings, while lower heights will lead to decreased SO_2 loadings. Although precipitation plays some role in higher and lower loadings, the major meteorological factor seems to be heights. Higher heights lead to stagnant air. This stagnant air allows for the loadings to have a longer lifetime in the region and not be able to disperse as it normally would. Winter 2012, with the same height field as winter 2008 and drier conditions, should lead to similar or higher loadings. However, winter 2012 loadings were lower. Also, winter 2013, though similar in heights to winter 2009 and wetter should lead to similar observed loadings to winter 2009. However, winter 2013 loadings were higher. Since winters 2012 and 2013 are not what we expected when comparing them to winters 2008 and 2009, we look to explore other meteorological factors that can attribute to these higher loading events.

4.2. OMI-based SO_2 decadal change and air pollution meteorology

Most of eastern China's SO_2 loadings are found between 112° and 122°E and 34°-40°N, as observed in the 10-year winter average of OMI SO_2 (Fig. 2A). From the decade worth of data obtained from OMI, we broke down the data into two, five-year periods; (1) 2006–2010 and (2) 2011–2015, to observe changes in SO_2 loadings since the installation of flue-gas desulfurization devices in power plants. These devices have been regulated by the Chinese government since 2006. During winters of 2006–2010, (Fig. 2C), the

average SO_2 loading was 0.77 DU with a maximum loading of 1.76 DU for the region. For winters of 2011–2015, (Fig. 2D), the average decreased to 0.55 DU (29.1% less) and the maximum loading decreased to 1.28 DU (27.4% less). The highest local loadings are located to the east of the Taihang Mountains along the border between Shanxi and Hebei provinces (Fig. 2). Most of this area is around 1.0 DU during winters 2006–2010 and was reduced to around 0.7 DU during 2011–2015. We checked to see if meteorological conditions had made a significant difference during the two time periods and found the 850 hPa heights and precipitation were near climatological averages (not shown) for both time periods. Our findings are similar to those found by Lu et al. (2010), where they also found reductions to be the most significant over eastern China.

During the decade of data from OMI, we next broke down the SO_2 data and correlated a climatological average and the top 10% maxima of SO_2 data days with mean meteorological conditions. These meteorological factors include: (1) 850 hPa heights, (2) 850 hPa temperatures, (3) 850 hPa relative humidities, (4) 850 hPa wind speeds, and (5) surface pressures. We were able to calculate a mean of the top 10% (Fig. 3), climatological average (Fig. 4) and a difference between the two (Fig. 5) for each grid box and contoured those results. Here we define the climatology for SO_2 as the 870 days of data from OMI. It should be noted that during the period, not every grid box has a data value for all 870 days, meaning, a grid box is averaged over the total number of days there are data values in that grid box and each value must be greater than 0 DU.

First, we calculate the conditions for the top 10% SO_2 days. The mean SO_2 (Fig. 3A), has high loadings around the province of Shanxi, with a maximum loading of almost 4 DU. This region has many coal power plants that help contribute to the higher maxima that we found. Surface pressures (Fig. 3C) are around 1000 hPa over eastern China and decreases over the mountains to the northwest.

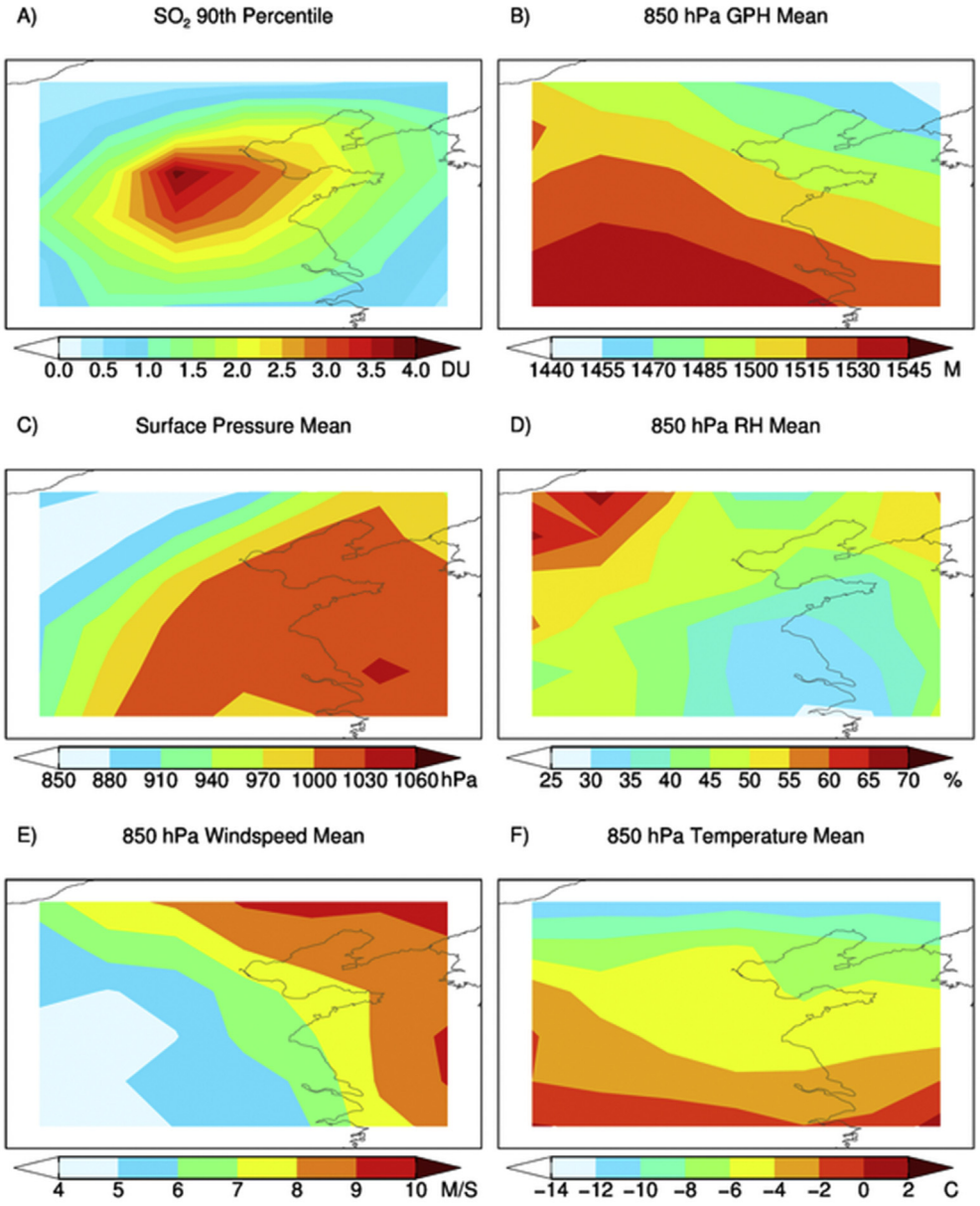

Fig. 3. (A) spatial distribution of the average of top 10% of OMI SO_2 amounts for each 2.5° × 2.5° grid box during winters of 2006–2015. (B)–(F) is similar to (A), but for each grid box, respectively show the average of geopotential height (GPH, in meter) at 850 hPa, surface pressure (in hPa), and 850 hPa relative humidity, wind speed, and temperature data corresponding to the days that have the top 10% SO_2 amount for that grid box.

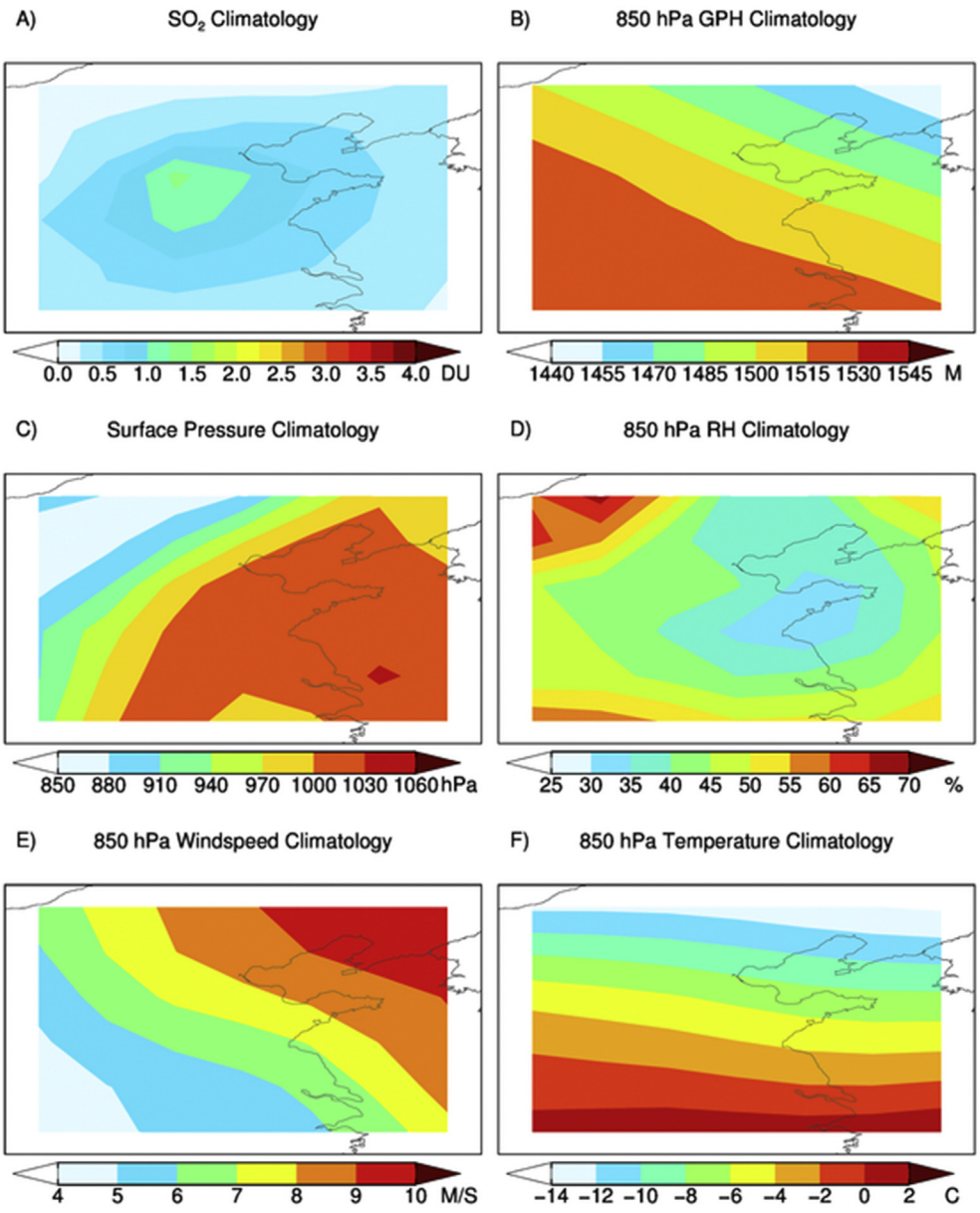

Fig. 4. Similar as Fig. 3, but shows the climatology or the average of variables for each 2.5° × 2.5° grid box in all winter days that have valid data for the corresponding variable during 2006–2015.

The 850 hPa heights (Fig. 3B) are around 1530 m in southern and eastern China to around 1440 m over northeastern China. 850 hPa relative humidities (Fig. 3D) are mostly between 30 and 50%, with higher values above 50% to the northwest, because of the mountains. The 850 hPa wind speeds (Fig. 3E) are between 4 and 10 m/s and the 850 hPa temperatures are relatively cold between −2 °C and −8 °C. These meteorological conditions play a major part in contributing to the high loading top 10% SO_2 days. The higher heights indicate there is a stronger high pressure system over southern and eastern China. The majority of maxima SO_2 loadings occur in areas of higher heights and lower wind speeds. Temperature and relative humidity are also cold and dry, meaning that we do not expect wet deposition to take place, thus inhibiting the removal of SO_2.

Second, we calculate the climatological conditions. The climatology (Fig. 4A) shows that NCP SO_2 loadings are greater than 0.5 DU, with the highest loading greater than 1.25 DU. Our climatology of surface pressure (Fig. 4C), when comparing to the mean top 10% loading days (Fig. 3C), is nearly identical. We expected this, as surface pressures did not vary as greatly as other meteorological conditions. The climatological 850 hPa heights, (Fig. 4B), are also nearly identical to the 1981–2010 height climatology (Fig. 1F) as expected. The 850 hPa relative humidity climatological values (Fig. 4D) are slightly drier than the top loading days (Fig. 3D), and the drier area has shifted significantly northwestward. The 850 hPa wind speeds (Fig. 4E) also show similar wind speeds to the top 10% loading mean conditions (Fig. 3E), however, lower speeds are found where the highest area loadings are located. Meanwhile, the 850 hPa temperature gradients, (Fig. 4F), varies greatly compared to the top 10% conditions (Fig. 3F).

Finally, we calculate the difference between the top 10% and the climatological conditions. The area of greatest concern for SO_2 (Fig. 5A), is the area greater than 0.5 DU, indicating that this area is continuously exposed to health risks using the criteria set by the

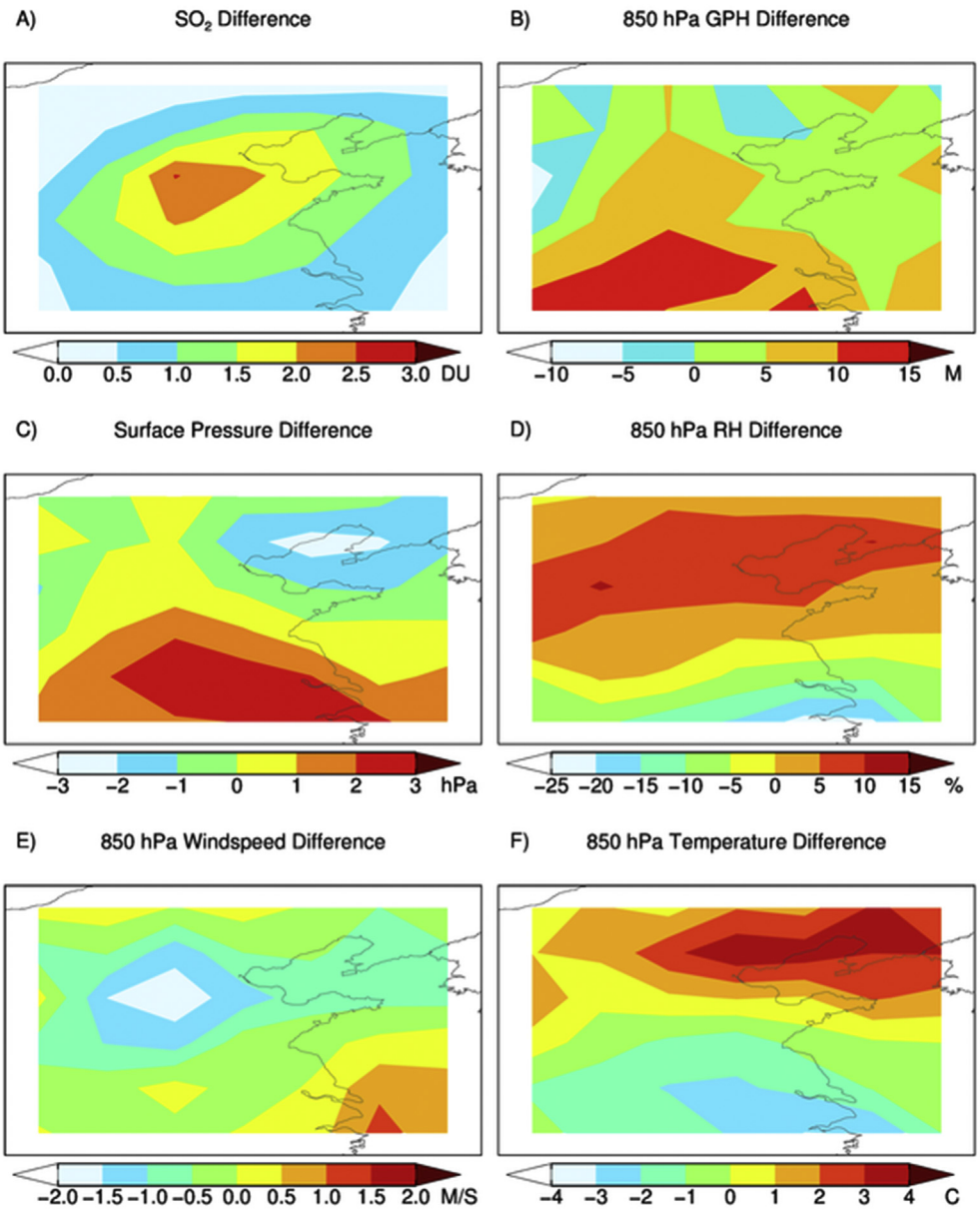

Fig. 5. Same as Fig. 3 but shows the difference between Fig. 3 and Fig. 4.

WHO (2001). Surface pressure differences (Fig. 5C) show no indication of having an impact on SO_2 loadings. 850 hPa height differences, (Fig. 5B), reveal that areas of higher heights will lead to higher loadings in SO_2. 850 hPa wind speeds (Fig. 5E) may be the driving force behind high SO_2 loadings. Comparing wind speeds and SO_2 loadings, there are clear indications that wind speed influences SO_2 loadings. The wind that is needed to displace the SO_2 out of the region, over the ocean, has decreased, allowing for SO_2 loadings to build over the NCP. The 850 hPa relative humidity values (Fig. 5D) and the 850 hPa temperatures (Fig. 5F) all show increases during the higher SO_2 loadings, suggesting that one meteorological parameter may not be the main factor for a higher or lower SO_2 loading, and the interactions with multiple parameters could increase the contributions.

4.3. Sensitivity analysis of meteorological impacts on SO_2

GEOS-Chem simulations are conducted for winters of 2009, 2012 and 2013 with a 100% default emission (Fig. 6). We define 2009 as a low SO_2 year, 2012 as a high year and 2013 intermediate year. These definitions are based on our results found in Fig. 1. Regardless of the year, a large area of SO_2 loadings, greater than 2.0 DU, are located over the Shanxi province (Fig. 6A–C). However, in 2012 and 2013, this area extends northeastward into the Hebei province and south/southwestward into the Shaanxi, Henan, Hubei and Chongqing provinces. Overall, the model-simulated distributions of SO_2 are consistent with what OMI observed in Fig. 1, showing overall low SO_2 loadings in 2009. However, a direct comparison between model and OMI SO_2 loadings needs the consideration of other factors such as spatial and temporal sampling characteristics of OMI as well as the averaging kernel used in the OMI SO_2 retrievals (Lee et al., 2009). Overall, past studies have shown GEOS-Chem has a high fidelity in simulating the distribution and transport of SO_2, and we refer readers to the work by Wang et al. (2012) and references therein. Our aim here is to use the GEOS-Chem model results to assess the meteorological impacts on

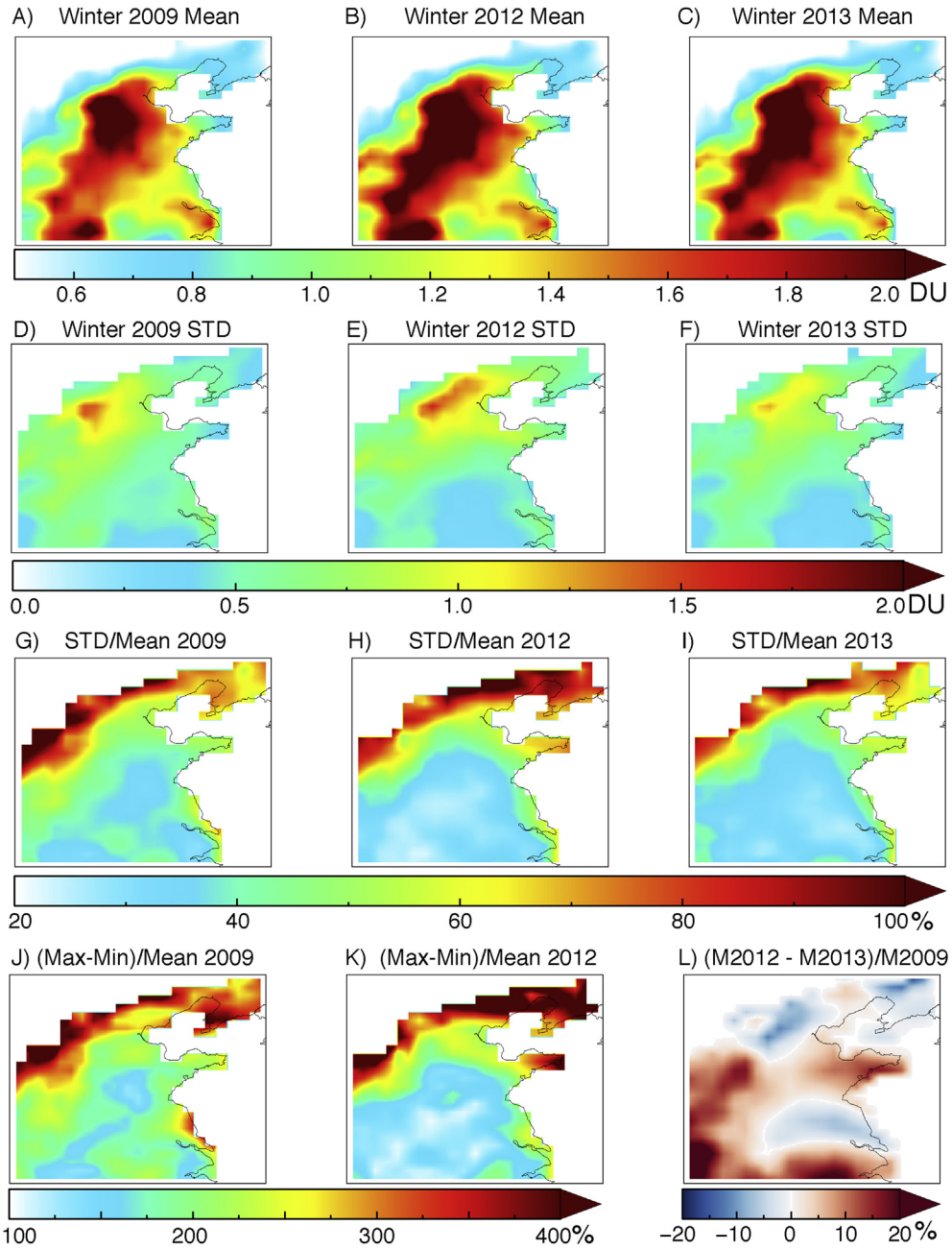

Fig. 6. A–C: Mean of columnar SO_2 amounts simulated by GEOS-Chem for the winters of 2009, 2012 and 2013, respectively. D–F: similar as A–C, however, for standard deviation. G–I: similar as D–F, however, for relative variation (standard deviation with respect to the mean). J–K: the range of SO_2 with respect to the mean for winters of 2009 and 2012, respectively. L: change of mean SO_2 between 2012 and 2013 with respect to the mean of 2009.

SO_2.

Within each year, the variability of columnar SO_2 in winter (quantified as standard deviation in Fig. 6D–F) is normally less than 1.5 DU, with larger values corresponding to the large values of columnar SO_2 itself. However, this correspondence is not linear; contrast between means (Fig. 6A–C) and standard deviations (Fig. 6D–F) show that locations with higher variabilities are indeed on the border between Hebei and Shanxi provinces, closer to the edge of the highest SO_2 loadings. The regions with large relative variabilities (or standard deviations divided by means, Fig. 6G–I) are those regions that do not have SO_2 sources, nevertheless are affected by the transport of SO_2 from the source region. Overall, in regions with large mean SO_2, the relative variabilities are often within 40%, which contrasts with those downwind regions where relative variabilities are larger than 60%.

To gain insights about possible ranges of SO_2 loadings with respect to the means, Fig. 6J–K shows the differences between maximum and minimum SO_2 loadings divided by the mean at each grid cell for winters of 2009 and 2012 respectively. The patterns are similar to relative variability (Fig. 6G–H), indicating higher SO_2 regions with a possible range of less than 300% and lower SO_2 regions with a possible range of larger than 350%. The range of SO_2 change appears to be smaller in 2012 than in 2009.

Change of meteorological conditions in different years can yield a change of winter-mean SO_2 loadings at different locations within ±20%, as shown in Fig. 6L. Further comparisons of frequency of

columnar SO_2 loadings in winters of different years show variations (Fig. 8A–C). For example, the data points of SO_2 loadings of less than 1.0 DU indicate that the largest frequency (51.1%) is in 2009, while the lowest frequency (47.2%) is in 2013. In comparison, the data points of SO_2 loadings larger than 3 DU show the largest frequency (3.4%) in 2012 and comparable frequency (2.7%) in 2009 and (2.6%) in 2013.

Fig. 7 presents a similar analysis to Fig. 6, however, for SO_2 loadings in the surface model layer (~100 m). While the distribution of surface SO_2 loadings resembles that of columnar SO_2 loadings, significant differences are also evident. In particular, surface SO_2 loadings are found to be largest in 2009 (Fig. 7A vs. B and C), which contrasts with the columnar loading that is smallest in 2009 (Fig. 6A vs. B and C). In terms of variability (Fig. 7D–F), the surface SO_2 loadings are within 0.25 DU and are smaller than its counterparts in the column, and hence the geographic distribution appears to be similar; comparable findings hold for relative variability (Fig. 7G–I) and relative range of change (Fig. 7J–K). However, the

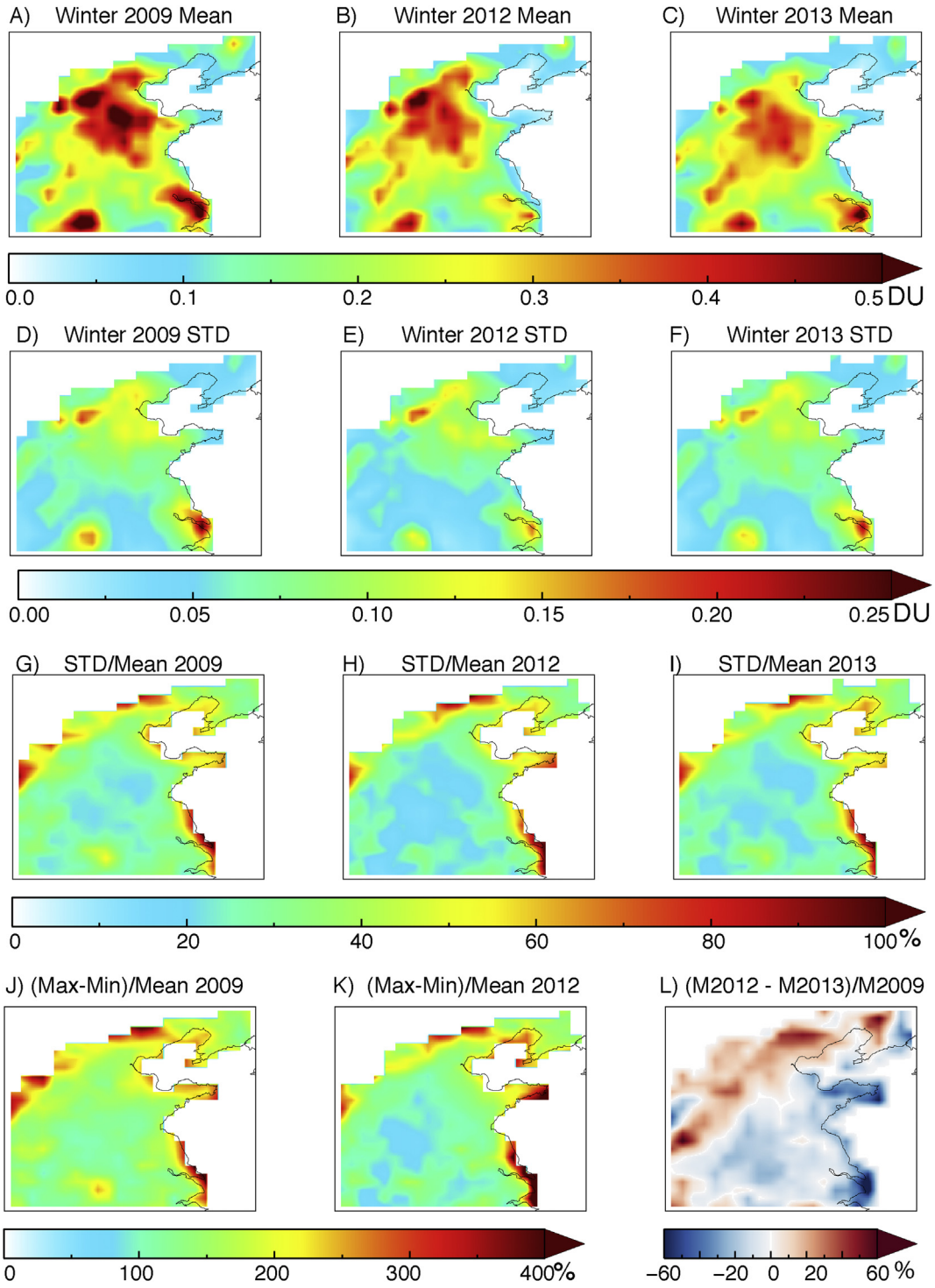

Fig. 7. Same as Fig. 6, but for SO_2 amount in the surface layer of the model.

mean of surface SO_2 appears to be more sensitive to the year-to-year change of meteorological conditions and can be up to ±60% (Fig. 7L), a factor of three larger than the counterparts of columnar SO2 loadings (Fig. 6L).

The distribution of surface SO_2 loading frequencies, shown in Fig. 8D–F for winters of 2009, 2012, and 2013, further reveals that winter 2009 is indeed equally polluted as 2013, with 41.4% of data points in the range of larger than 0.2 DU in the surface layer. In comparison, the winter of 2012 is less polluted with 39.3% of data points for SO_2 loadings larger than 0.2 DU. The contrast between Fig. 8A–C (showing most polluted in 2012 and least amount in 2013 in terms of relative percentage of data points with values larger than 2 DU) and Fig. 8D–F (showing 2012 being less polluted) reveals that the columnar SO_2 may not be representative of surface SO_2 loadings during high SO_2 episodes, highlighting the importance of meteorological conditions in regulating the vertical profile of SO_2, suggesting complications of using satellite-based columnar SO_2 to characterize the SO_2 air quality at the surface during high SO_2 episodes.

Further investigation of the effect of changing SO_2 emission on atmospheric SO_2 distribution is conducted by reducing the GEOS-Chem default SO_2 emission by 50% and then running GEOS-Chem for 2009, 2012, and 2013 (Fig. 9). It reveals that for each winter, the response of the seasonal mean columnar SO_2 loadings to the reduction of SO_2 emissions exhibit similar spatial distributions, regardless of the difference in meteorological conditions; the response, quantified in terms of relative change with respect to the mean without SO_2 emission reduction, appears to be semi-linear with a range of 45–55%. Indeed, in the high SO_2 emission regions (in Hebei, Tanjing, and Beijing), the relative change of atmospheric SO_2 columnar loadings are 50%, a nearly exact linear response to the 50% reduction of SO_2 emissions. To the south of the high SO_2 emission regions, the SO_2 relative changes range from 50 to 54%, indicating that the reduction of SO_2 emissions can lead to somewhat disproportionately larger reductions (up to 4%) in atmospheric SO_2 total loadings. In contrast, over the northern regions, the SO_2 relative change range is 46%–50%, indicating that the response of atmospheric SO_2 loadings to the reduction of SO_2 emission is mostly linear or the non-linear effect is minor (up to 4%). Overall, as a whole, the total amount of SO_2 in the atmosphere appears to be a linear response to the change of SO_2 emission, at least in the seasonal averages.

Further analysis, however, indicates that the response of surface SO_2 amounts are highly nonlinear with respect to the change of SO_2 emissions (Fig. 9D–F). For a 50% reduction of emission, the response is in the range of 20–80% and exhibits different spatial distributions in different years (Fig. 9D–F). In high SO_2 emission regions, the reduction of 50% emission leads to a 30% reduction of atmospheric SO_2 near the surface in 2009, however, a 70% reduction in 2012, and nearly 50% in 2013 (Fig. 9D–F respectively). Depending on the region, the year-to-year change of meteorological conditions can result up to ±50% variability in the response (or relative change, Fig. 9G–I). This nonlinear relationship between near-surface SO_2 and SO_2 emission can also be seen by comparing Fig. 8D–F with Fig. 8G–I, showing the frequency of distribution of near surface SO_2 for 100% and 50% emission, respectively. For example, 32.2% of the data points have SO_2 amounts in the range of 0.2–0.4 DU in 2012 for 100% emission (Fig. 8E). If the near-surface SO_2 and SO_2 emission has a linear relationship, the reduction of emission by 50% would also lead to the same portion (32.2%) of data

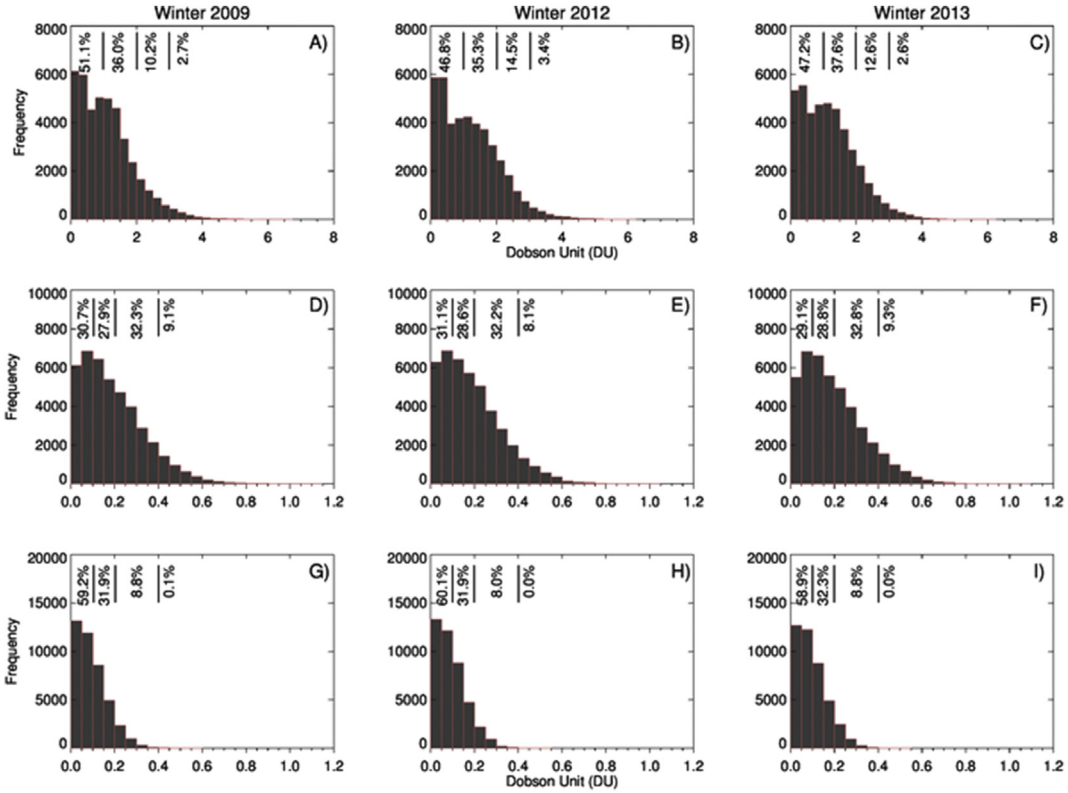

Fig. 8. Frequency of GEOS-Chem simulated hourly columnar (top row) and surface layer (middle row) SO_2 amounts at each model grid box over the continent in the model domain for 2009 (left column), 2012 (middle column), and 2013 (right column), respectively. The bottom row is for surface layer SO_2 amounts simulated by GEOS-Chem with a 50% reduction of SO_2 emission. The relative percentages of the number of data points at every 1 DU interval up to 3 DU and more than 3 DU are shown on the top left of each panel in the top row, and the relative percentages of the number of data points in range of 0 – 0.1 DU, 0.1 – 0.2 DU, 0.2 – 0.4 DU, and more than 0.4 DU are shown on the top left of each panel in middle and bottom row.

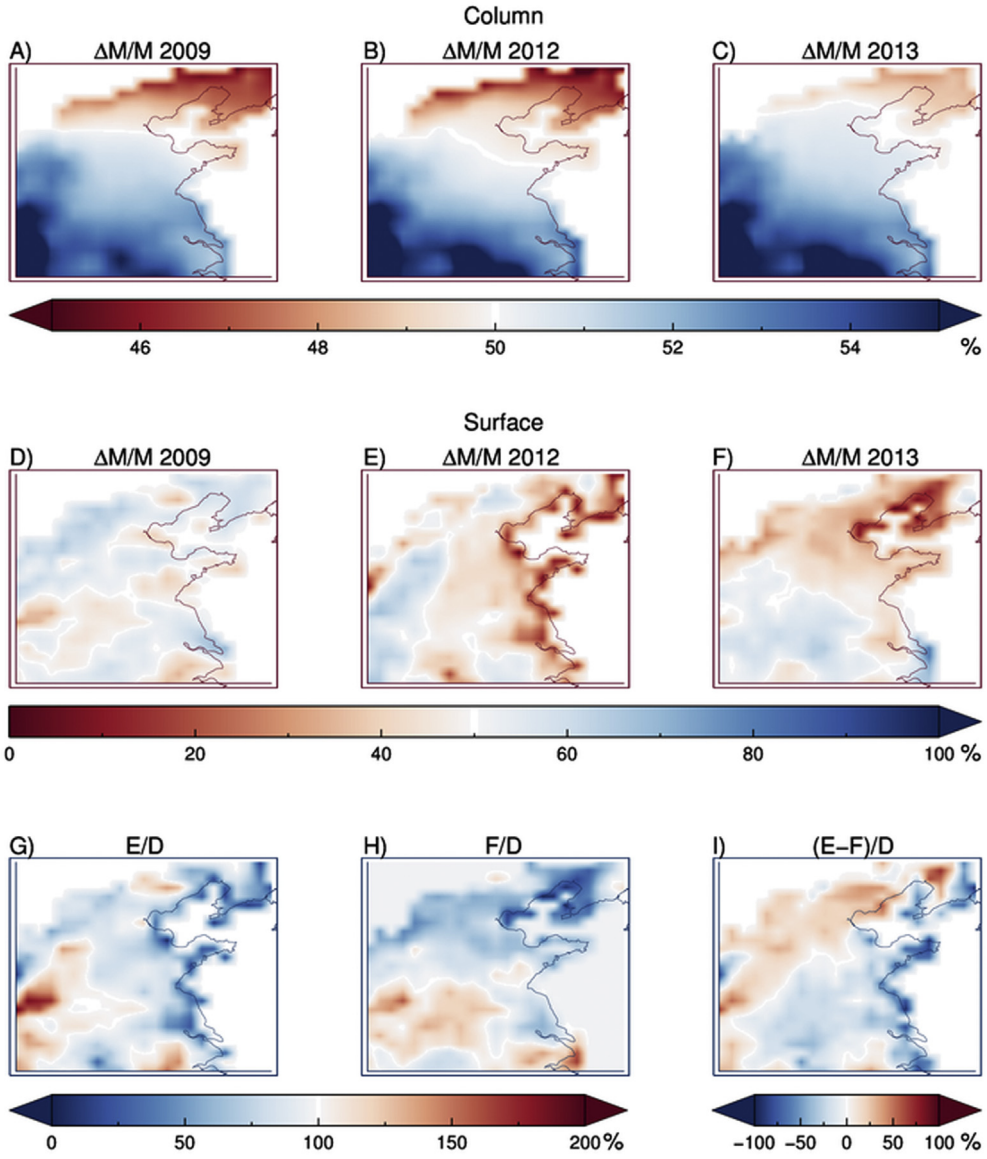

Fig. 9. Relative change of winter mean (M) SO_2 amounts (ΔDM/M) in response to the 50% reduction SO_2 emission for 2009, 2012 and 2013 respectively. Top row shows the relative change for columnar SO_2 amounts while the second row from the top for SO_2 amounts at the surface. F and G show the ratio of relative change in 2009 and 2013 with respect to the counterpart in 2012 (e.g., data values in panel D and E divided by panel C), respectively. H shows the ratio of difference of relative change between 2012 and 2009 with respect to relative change in 2012. Lines in white color show the isopleths at 0%, 50%, and 100% for A–E, F–G, and H, respectively.

points for SO_2 amounts in range of 0.1–0.2 DU; however, the simulation shows this portion is 31.9%, suggesting a non-linear relationship. It is interesting to note that in all three years, reduction of emissions appears to in proportionally suppressing the more extreme polluted cases; for near-surface SO_2 loadings larger than 0.4 DU (in simulations with 100% emission), the corresponding portion of data points are 9.1% 8.1% and 9.3% in 2009, 2012, and 2013 respectively, which are all higher than their counterparts in the simulation with 50% emission (e.g. 8.9, 8% and 8.8% of data points with SO_2 values larger than 0.2 DU).

5. Summary

Using OMI and GEOS-Chem, we studied the characteristics of how meteorological conditions affect SO_2 distributions in the NCP during the winters of 2006–2015. The main conclusions are as follows:

- OMI SO_2 data show that atmospheric SO_2 loadings in China have drastically decreased by 30% from the 2006–2010 period to the 2011–2015 period. This can be attributed to the installation of flue-gas desulfurization devices.
- High SO_2 days are found to be associated with stagnant, warm and moist air masses that average 1–2 hPa higher in surface pressure, as well as 850 hPa level increases in geopotential height of 5–10 m, 1–3 °C warmer temperatures, 10%–15% higher relative humidities, and up to 2 m s^{-1} slower wind speeds.
- Numerical experiments with GEOS-Chem model simulations reveal that the relative change of columnar distribution of SO_2 in response to a change of meteorological conditions and seasonal averaged emissions are normally within 10%–20%, suggesting a high consistence or semi-linear relationship between columnar SO_2 observations and SO_2 emissions are expected. In contrast, the relative change of SO_2 loadings near the surface exhibit stronger dependence on (surface) meteorological conditions

and thereby, a non-linear relationship with respect to the change of emissions; the year-to-year change of surface SO_2 amounts due to change of meteorological conditions can be up to 20–30% and the response to the change of emissions can deviate from linear relationship by up to 50%. It is concluded that the climatology of columnar SO_2 amounts is not representative and sometime can be opposite to the climatology of surface SO_2 loadings.

These findings underscore the importance of considering the role of meteorological conditions in the application of satellite-based SO_2 data to study air pollution events. Through a combined use of meteorological data with satellite-based SO_2 data, an observation-based air pollution climatology can be revealed and studied. Unlike the climatology for meteorological variables, the climatology for SO_2 air pollution can be affected by the change of emissions. Given that the emission of SO_2 in our study region has been declining in the past decade, there is a possibility that the top 10% polluted days might be more concentrated in the first half of the past decade. However, quantifying such a possibility is difficult because of the year-to-year change of meteorological conditions that alone can lead to the change of seasonal mean SO_2 loading by ±20% (Fig. 6L), which is significant enough to offset the variation of SO_2 due to year-to-year change of SO_2 emission. For example, in Beijing, we found that the largest SO_2 loading over Bejing occurred in 2012, while the second and third largest occurred in 2006 and 2009, respectively. Nevertheless, our sampling of heavily polluted days can be affected by many factors, not only emission and meteorological conditions, but also instrument's spatial and temporal coverages. Since OMI's SO_2 data record only starts in 2004 and with its limited spatial and temporal sampling due to the row anomaly, a longer SO_2 data record from space with high density in spatial and temporal sampling are needed, and thus would reveal insights from a SO_2 pollution climatology and associated meteorological conditions.

Acknowledgement

This work. was supported by NASA Aura Science program (grant #: NNX14AG01G managed by Dr. Ken Jucks), Applied Science Program (grant #: NNX15AC28A managed by Dr. John Haynes), and ACMAP program (grant #: NNX15AC30G managed by Dr. Richard Eckman) and by Holland Computing Center and Office for Research and Economic Development in University of Nebraska-Lincoln. We thank Mr. Curtis Walker for proofreading this article.

References

Afe, O.T., Richter, A., Sierk, B., Wittrock, F., Burrows, J.P., 2004. BrO emission from volcanoes: a survey using GOME and SCIAMACHY measurements. Geophys. Res. Lett. 31, L24113. http://dx.doi.org/10.1029/2004GL020994.

Bey, I., Jacob, D.J., Yantosca, R.M., Logan, J.A., Field, B.D., Fiore, A.M., Li, Q., Liu, H.Y., Mickley, L.J., Schultz, M.G., 2001. Global modeling of tropospheric chemistry with assimilated meteorology: model description and evaluation. J. Geophys. Res. 106, 23073–23095. http://dx.doi.org/10.1029/2001JD000807.

Bridgman, H.A., Davies, T.D., Jickells, T., Hunova, I., Tovey, K., Bridges, K., Surapipith, V., 2002. Air pollution in the Krusne Hory region,Czech Republic during the 1990s. Atmos. Environ. 36, 3375–3389. http://dx.doi.org/10.1016/S1352-2310(02)00317-5.

Carn, S.A., Yang, K., Prata, A.J., Krotkov, N.A., 2015. Extending the long-term record of volcanic SO2 emissions with the Ozone Mapping and Profiler Suite nadir mapper. Geophys. Res. Lett. 42, 925–932. http://dx.doi.org/10.1002/2014GL062437.

Chan, C.K., Yao, X., 2008. Air pollution in mega cities in China. Atmos. Environ. 42, 1–42. http://dx.doi.org/10.1016/j.atmosenv.2007.09.003.

Cuhadaroglu, B., Demirci, E., 1997. Influence of some meteorological factors on air pollution in Trabzon City. Energy Build. 3, 179–184.

Fiore, A.M., Naik, V., Spracklen, D.V., Steiner, A., Unger, N., Prather, M., Bergmann, D., Cameron-Smith, P.J., Cionni, I., Collins, W.J., Dalsøren, S., Eyring, V., Folberth, G.A., Ginoux, P., Horowitz, L.W., Josse, B., Lamarque, J.F., MacKenzie, I.A., Nagashima, T., O'Connor, F.M., Righi, M., Rumbold, S.T., Shindell, D.T., Skeie, R.B., Sudo, K., Szopa, S., Takemura, T., Zeng, G., 2012. Global air quality and climate. Chem. Soc. Rev. 41 (19), 6663–6683.

He, H., Li, C., Loughner, C.P., Li, Z., Krotkov, N.A., Yang, K., Wang, L., Zheng, Y., Bao, X., Zhao, G., Dickerson, R.R., 2012. SO2 over central China: measurements, numerical simulations and the tropospheric sulfur budget. J. Geophys. Res. 16, D00K37. http://dx.doi.org/10.1029/2011JD016473.

Ilten, N., Selici, A.T., 2008. Investigating the impacts of some meteorological parameters on air pollution in Balikesir, Turkey. Environ. Monit. Assess. 140, 267–277.

Kalnay, E., Kanamitsu, M., Kistler, R., Collins, W., Deaven, D., Gandin, L., Iredell, M., Saha, S., White, G., Woollen, J., Zhu, Y., Leetmaa, A., Reynolds, R., Chelliah, M., Ebisuzaki, W., Higgins, W., Janowiak, J., Mo, K.C., Ropelewski, C., Wang, J., Jenne, Roy, Joseph, Dennis, 1996. The NCEP/NCAR 40-Year reanalysis Project. Bull. Amer. Meteor. Soc. 77, 437–471.

Krotkov, N. A., S. A. Carn, A. J. Krueger, P. K. Bhartia, and K. Yang, 2006: band residual difference algorithm for retrieval of SO_2 from the Aura ozone monitoring instrument (OMI). IEEE Trans. Geoscience Remote Sens., 44, 1259–1266, doi: 10.1109/TGRS.2005.861932.

Krotkov, N.A., McClure, B., Dickerson, R.R., Carn, S.A., Li, C., Bhartia, P.K., Yang, K., Krueger, A.J., Li, Z.L., Levelt, P.F., Chen, H., Wang, P., Lu, D., 2008. Validation of SO_2 retrievals from the ozone monitoring instrument over NE China. J. Geophys. Res. 113, 1–13. http://dx.doi.org/10.1029/2007JD008818.

Krotkov, N.A., Li, C., Leonard, P., 2015. OMI/Aura Sulfur Dioxide (SO2) Total Column L3 1 Day Best Pixel in 0.25 Degree X 0.25 Degree V3, Version 003. Goddard Earth Sciences Data and Information Services Center (GES DISC), Greenbelt, MD, USA. http://dx.doi.org/10.5067/Aura/OMI/DATA3008. Accessed 4 May 2015.

Lee, C., Martin, R.V., van Donkelarr, A., O'Byrne, A., Krotkov, N., Richter, A., Huey, L.G., Holloway, J.S., 2009. Retrieval of vertical columns of sulfur dioxide from SCIAMACHY and OMI: air mass factor algorithm development, validation, and error analysis. J. Geophys. Res. 114, D22303. http://dx.doi.org/10.1029/2009JD012123.

Lee, C., Richter, A., Burrows, J.P., 2008. SO_2 retrieval from SCIAMACHY using the Weighting Function DOAS (WFDOAS) technique: comparison with standard DOAS retrieval. Atmos. Chem. Phys. 8, 6137–6145. http://dx.doi.org/10.5194/acp-8-6137-2008.

Lee, C., Martin, R.V., Donkelarr, A.V., Lee, H., Dickerson, R.R., Hains, J.C., Krotkov, N., Richter, A., Vinnikov, K., Schwab, J.J., 2011. SO2 emissions and lifetimes: estimates from inverse modeling using in situ and global, space-based (SCIAMACHY and OMI) observations. J. Geophys. Res. 116, 1–13. http://dx.doi.org/10.1029/2010JD014758.

Levelt, P.F., van den Oord, G.H.J., Dobber, M.R., Mälkki, A., Visser, H., Vries, J.D., Stammes, P., Lundell, J.O.V., Saari, H., 2006. The ozone monitoring instrument. IEEE Trans. Geoscience Remote Sens. 44, 1093–1101.

Li, C., Zhang, Q., Krotkov, N.A., Streets, D.G., He, K., Tsay, S.-C., Gleason, J.F., 2010. Recent large reduction in sulfur dioxide emissions from Chinese power plants observed by the Ozone Monitoring Instrument. Geophys. Res. Lett. 37, L08807.

Li, C., Joiner, J., Krotkov, N.A., Bhartia, P.K., 2013. A Fast and sensitive new satellite SO_2 retrieval algorithm based on principal component analysis: application to the ozone monitoring instrument. Geophys. Res. Lett. 40 http://dx.doi.org/10.1002/2013GL058134.

Lu, Z., Streets, D.G., Zhang, Q., Wang, S., Carmichael, G.R., Cheng, Y.F., Wei, C., Chin, M., Diehl, T., Tan, Q., 2010. Sulfur dioxide emissions in China and sulfur trends in East Asiasince 2000. Atmos. Chem. Phys. 10, 6311. http://dx.doi.org/10.5194/acp-10-6311-2010.

Lu, Z., Zhang, Q., Streets, D.G., 2011. Sulfur dioxide and primary carbonaceous aerosol emissions in China and India, 1996-2010. Atmos. Chem. Phys. 11, 9839–9864. http://dx.doi.org/10.5194/acp-11-9839-2011.

Olivier, J.G.J., Berdowski, J.J.M., 2001. Global emissions sources and sinks. Clim. Syst. 33–78.

Park, R.J., Jacob, D.J., Field, B.D., Yantosca, R.M., 2004. Natural and transboundary pollution influences on sulfate-nitrate-ammonium aerosols in the United States: implications for policy. J. Geophys. Res. 109, 1–20. http://dx.doi.org/10.1029/2003JD004473.

Richter, A., Wittrock, F., Burrows, J.P., 2006. SO_2 measurements with SCIAMACHY. In: Proceeding of Atmospheric Science Conference, Frascati, Italy. ESA/ESRIN, Noordwijk, Netherlands, 8–12 May, ESA Publ. SP-628.

Smith, S.J., van Aardenne, J., Klimont, Z., Andres, R.J., Volke, A., Delgado Arias, S., 2011. Anthropogenic sulfur dioxide emissions: 1850-2005. Atmos. Chem. Phys. 11, 1101–1116. http://dx.doi.org/10.5194/acp-11-1101-2011.

Wang, J., Park, S., Zeng, J., Ge, C., Yang, K., Carn, S., Krotkov, N., Omar, A.H., 2013. Modeling of 2008 Kasatochi volcanic sulfate direct radiative forcing: assimilation of OMI SO2 plume height data and comparison with MODIS and CALIOP observations. Atmos. Chem. Phys. 13, 1895–1912. http://dx.doi.org/10.5194/acp-13-1895-2013.

WHO, 2001. Environment and People's Health in China [Available online at: http://www.wpro.who.int/environmental_health/documents/docs/CHNEnvironmentalHealth.pdf].

Xue, D., Yin, J., 2013. Meteorological influence on predicting surface SO2 concentration from satellite remote sensing in Shanghai, China. Environ. Monit. Assess. 186, 2895–2906. http://dx.doi.org/10.1007/s10661-013-3588-2.

Yang, K., Krotkov, N.A., Krueger, A.J., Carn, S.A., Bhartia, P.K., Levelt, P.F., 2007. Retrieval of large volcanic SO_2 columns from the Aura ozone monitoring instrument: comparison and limitations. J. Geophys. Res. 112, D24S43. http://dx.doi.org/10.1029/2007JD008825.

Yang, K., Dickerson, R., Carn, S., Wang, J., Ge, C., 2013. First observations of SO2 from

Suomi NPP OMPS: widespread air pollution events over China. Geophys. Res. Lett. 40, 4957–4962. http://dx.doi.org/10.1002/grl.50952.

Zhang, Q.Q., Yang, Y., Ma, Q., Yao, Y., Xie, Y., He, K., 2015. Regional differences in Chinese SO2 emission control efficiency and policy implications. Atmos. Chem. Phys. 15, 6521–6533. http://dx.doi.org/10.5194/acp-15-6521-2015.

Zhang, Q., Streets, D.G., Carmichael, G.R., He, K.B., Huo, H., Kannari, A., Klimont, Z., Park, I.S., Reddy, S., Fu, J.S., Chen, D., Duan, L., Lei, Y., Wang, L.T., Yao, Z.L., 2009. Asian emissions in 2006 for the NASA INTEX-B mission. Atmos. Chem. Phys. 9, 5131–5153.

Zhang, X., van Geffen, J., Liao, H., Zhang, P., Lou, S., 2012. Spatiotemporal variations of tropospheric SO_2 over China by SCIAMACHY observations during 2004–2009. Atmos. Environ. 60, 238–246. http://dx.doi.org/10.1016/j.atmosenv.2012.06.009.